PROCEEDINGS OF SCIENCE

Plans and Status of the Phase I Upgrade of the CMS Pixel Tracker

Hanno Perrey[*†]
Deutsches Elektronen-Synchrotron (DESY)
E-mail: hanno.perrey@desy.de

The silicon pixel detector is the innermost component of the CMS tracking system and plays a crucial role in the all-silicon CMS tracker.
While the current pixel tracker is designed for and performing well at an instantaneous luminosity of up to $1 \times 10^{34}\,\mathrm{cm}^{-2}\mathrm{s}^{-1}$, it can no longer be operated efficiently at significantly higher values.
Based on the strong performance of the LHC accelerator, it is anticipated that peak luminosities of two times the design luminosity are likely to be reached before 2018 and perhaps significantly exceeded in the running period until 2022, referred to as Phase I.
Therefore an upgrade is planed for the year-end technical stop in 2016: With a new pixel readout chip (ROC), an additional fourth layer, two additional endcap disks, and a significantly reduced material budget the upgraded pixel detector will be able to sustain the efficiency of the pixel tracker at the increased requirements imposed by high luminosities and pile-up.
In this contribution, the new design of the pixel detector along with its expected physics performance will be presented. Also, the results of first ROC beam tests will be reported.

22nd International Workshop on Vertex Detectors,
15-20 September 2013
Lake Starnberg, Germany

[*]Speaker.
[†]for the CMS Tracker Collaboration.

PoS(Vertex 2013)014

1. Introduction

The present pixel detector is a crucial component of the all-silicon CMS tracker [1, 2]. It was designed to record efficiently and with high precision the first three space-points near the interaction region, up to pseudorapidities[1] of ± 2.5, under operating conditions of $1 \times 10^{34}\,\mathrm{cm}^{-2}\mathrm{s}^{-1}$ instantaneous luminosity and 40 MHz bunch crossing frequency.

The current pixel detector consists of three barrel layers (BPIX) at radii of 4.4 cm, 7.3 cm and 10.2 cm, and two forward/backward disks (FPIX) at longitudinal positions of ± 34.5 cm and ± 46.5 cm and extending in radius from about 6 cm to 15 cm. The BPIX contains 48 million pixels covering a total area of $0.78\,\mathrm{m}^2$ and the FPIX has 18 million channels covering an area of $0.28\,\mathrm{m}^2$. These pixelated detectors produce 3-D measurements along the paths of the charged particles with single hit resolutions between $\sim 9\,\mu$m in r-ϕ and $\sim 20\,\mu$m in z.

2. Phase-I Upgrade Plans

Thanks to the impressive performance of the LHC machine, the original operating scenario, delivering an instantaneous luminosity of $1 \times 10^{34}\,\mathrm{cm}^{-2}\mathrm{s}^{-1}$ at 25 ns colliding bunch spacing and at 14 TeV center-of-mass energy, is likely to be achieved already in 2015. Under these conditions, CMS will experience an average of about 25 inelastic interactions per bunch crossing (referred to as event pile-up). Based on the excellent operation to date, and the upgrade plans for the LHC injector chain in 2018 to deliver high intensity and low emittance bunches, it is anticipated that peak luminosities of two times the design luminosity are likely to be reached before 2018 and perhaps significantly exceeded after the long shutdown in 2018.

While the current pixel tracker is designed for and performing well at an instantaneous luminosity of $1 \times 10^{34}\,\mathrm{cm}^{-2}\mathrm{s}^{-1}$, it can no longer be operated efficiently at significantly higher values: the pixel detector would suffer from inefficiencies due to readout-induced dead time, tracking inefficiencies or higher fake rates due to difficult pattern recognition, and effects of radiation damage built up over several years of operation. The combination of these effects would lead to unacceptable loss in sensitivity and physics reach. Additionally, from the standpoint of physics analyses, further improvements such as an additional pixel layer and a reduction of material are highly desirable to gain in acceptance and in impact parameter resolution.

Therefore, the goal of the Phase I upgrade [3] is to replace the present pixel detector with one that can maintain a high tracking performance at luminosities up to $2 \times 10^{34}\,\mathrm{cm}^{-2}\mathrm{s}^{-1}$ and pile-up up to and exceeding 50. The replacement is scheduled for the winter technical stop of 2016/2017. In order to minimize risk and to ensure that the installation procedure can be performed in the short time frame of a technical stop, the existing services such as power cables and optical fibers will be reused.

2.1 Sensor Technology

In case of the sensors, the design of the current detector will be kept for the upgrade: n^+-in-n sensors with $100 \times 150\,\mu\mathrm{m}^2$ size pixels (shown in figure 1), processed on 285 µm thick diffusion

[1] The pseudorapidity is defined as $\eta = -\ln\tan(\theta/2)$, where θ denotes the angle between a particle originating from the interaction point and the beam axis.

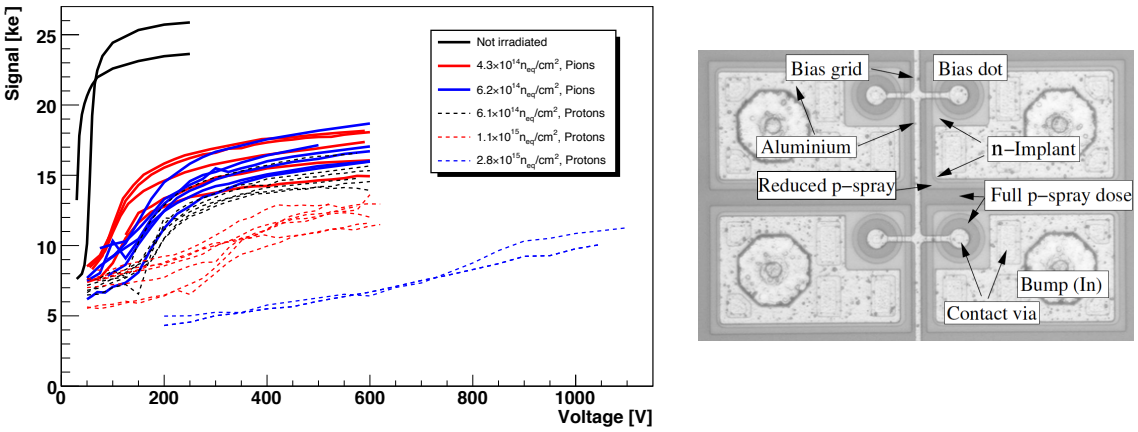

Figure 1: *Left:* Charge collection in non-irradiated and irradiated sensors with different doses and different particle types (sensors of $285 \pm 15\,\mu$m thickness). A ^{90}Sr source has been used for inducing signals in the sensor. *Right:* Photograph of four pixel cells in the same double column for BPIX

oxygenated float zone silicon using p-spray (BPIX) or p-stop (FPIX) for n-side isolation. This technology choice is known to be sufficiently radiation hard as demonstrated in figure 1 (*left*) showing the signal of non-irradiated and irradiated CMS pixel barrel sensor samples with different doses as function of the applied bias voltage [4]. The sensors were bump-bonded to read-out chips prior to their irradiation with either pions or protons.

Using a ^{90}Sr source to induce the signal, data could be taken with all samples, even the ones irradiated to the highest fluence of $2.8 \times 10^{15}\,\mathrm{n_{eq}/cm^2}$. This value well exceeds the fluence of $\sim 1.5 \times 10^{15}\,\mathrm{n_{eq}/cm^2}$ expected during the life time[2] of layer 1 BPIX. For all fluences smaller than $10^{15}\,\mathrm{n_{eq}/cm^2}$ the sensors clearly deplete and only little signal is gained for a bias larger than about 300 V. While for higher fluences, no clear saturation is visible even for the higher biases measured. At 600 V the sample with the highest fluence produces a signal of ~ 6000 electrons which is not sufficient for reliable operation with the present readout electronics, where the in-time threshold is around 3500 electrons.

However, this fluence exceeds the expected fluence for the layer 1 by almost a factor of two; furthermore, improvements to the read-out chip discussed in the following section significantly decrease the possible threshold to around 1500 electrons. Both these factors ensure that the layer 1 modules can be efficiently operated during the expected life time with a bias voltage not higher than 600 V.

2.2 Read-Out Chip Improvements

The basic operation of the read-out chip (ROC) is to store and output hit information for pixels with charge exceeding a set threshold. As illustrated by figure 2, the current ROC operates nearly dead-time free at low pixel hit rates but suffers from up to 4% data loss in layer 1 at the design

[2]The total fluence expected to be accumulated in the innermost layer during Phase 1 amounts to $\sim 3 \times 10^{15}\,\mathrm{n_{eq}/cm^2}$ corresponding to an integrated luminosity of $500\,\mathrm{fb}^{-1}$. However, a replacement of layer 1 is foreseen every $250\,\mathrm{fb}^{-1}$.

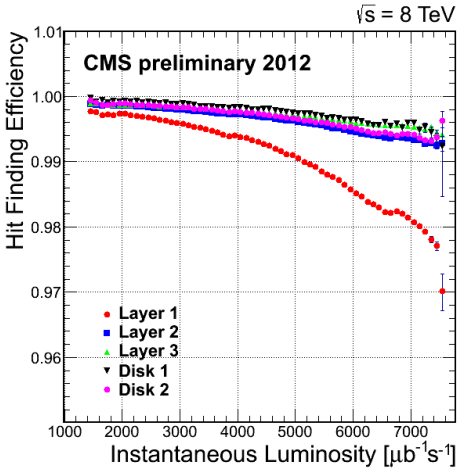

Figure 2: Pixel tracking performance measurements from 2012 data showing the average module hit efficiency as a function of the instantaneous luminosity for all layers and disks.

luminosity. However, at two times the design luminosity, the data loss increases to 16% and even to as much as 50% in the case of the LHC operating with bunch spacing of 50 ns.

This inefficiency is caused by limited buffering and latencies, the most important being overflows in time stamp and data buffers, speed limitation in the transfer of hits from the pixels to the double column periphery, and dead time of a double column while waiting to be read out. Furthermore, the bandwidth of the data links poses a limit to the data rate. To remedy these issues, significant improvements for the current ROC design are under development.

The new ROC is an evolution of the current architecture and is fabricated in the same 250 nm process. It features more data and timestamp buffer cells to prevent overflow at high hit occupancies, replaces the 40 MHz analog with a 160 MHz digital readout for twice the data throughput per optical fiber, and adds an additional buffered FIFO readout stage. As a result, for 25 ns operation of the LHC at highest Phase 1 luminosity of $2 \times 10^{34}\,\mathrm{cm}^{-2}\mathrm{s}^{-1}$, data loss due to dead time can be kept below 4.7% in the innermost layer[3], while it would amount to about 16% for the current detector.

Furthermore, the new ROC brings enhanced analog performance: reduced internal cross-talk and a faster pixel cell comparator allow for lower charge thresholds and the reduction of time-walk effects, respectively. These improvements result in a better and longer lasting performance of the pixel detector in the presence of radiation damage.

2.3 Detector Geometry & Material Budget

With more interactions per bunch crossing giving rise to additional hits in the tracking detectors, the pattern recognition becomes more difficult. At high pileup the processing of the tracking algorithms is one of the dominant contributions to the CPU time in both the High Level Trigger and the offline processing, and limits the data-taking rate. Under such conditions, the tracking efficiency can only be sustained at the expense of a higher level of fake tracks.

[3]For 50 ns LHC bunch structure or a mean of 100 pile-up events per bunch crossing, this inefficiency would be 6% for the upgraded ROC.[5]

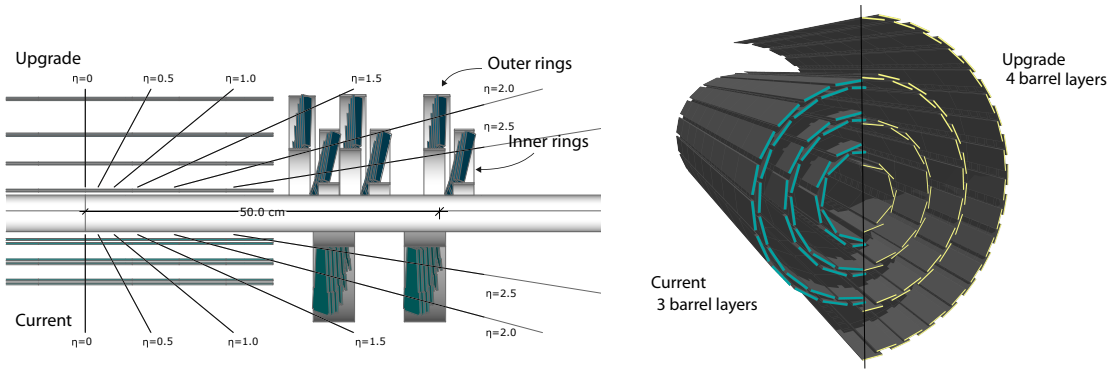

Figure 3: The conceptual layout for the Phase I upgrade pixel detector in $r-z$ view (left) and 3-D view (right) compared to the present detector design. The current 3-layer barrel (BPIX), 2-disk end cap (FPIX) system is replaced with a 4-layer barrel, 3-disk end cap system for four hit coverage. Additionally, the innermost layer 1 of the BPIX is moved closer to the interaction point.

Furthermore, particularly for higher values of the pseudorapidity, the current pixel detector contains a sizable amount of material. Photons and pions can be lost in this material due to conversion and nuclear interactions respectively, electrons will lose energy through bremsstrahlung, and charged particles will suffer scattering effects close to the main pp interaction point which can affect vertexing. These effects may contribute to additional confusion for track pattern recognition in a high pileup environment.

To mitigate the negative effects of pileup, the upgraded pixel detector will therefore feature an additional fourth barrel layer and one additional end cap disk on both sides. Figure 3 shows a schematic comparison of the new and present detector designs.

This detector geometry will provide four-hit coverage over the full acceptance range of $|\eta| < 2.5$, thus improving pattern recognition and track reconstruction. Furthermore, the radius of the innermost barrel layer will be reduced from 44 mm down to 29 mm, which will improve the physics performance of the pixel detector in terms of impact parameter resolution and vertex resolution. This makes a new smaller diameter beam pipe necessary which will be installed in the spring of 2014.

Since the extra pixel layer adds about $\sim 50\%$ to the total number of modules it could easily increase the total amount of material of the pixel detector. To avoid this, the upgraded detector, support, and services are redesigned to be lighter than the present system, using an ultra-lightweight support (shown on the right in figure 4) with CO_2 cooling, and especially by relocating much of the passive material, like the electronic boards and connectors, out of the tracking volume.

A comparison of the material budget for the current and Phase I pixel detectors was done by simulating neutrinos in the detector and summing the radiation length along a straight line at fixed values of pseudorapidity, η, originating from the interaction point. Figure 4 shows a comparison of the radiation length of the present and upgrade pixel detectors as a function of η. The green histogram represents the current pixel detector while the Phase I upgraded detector is given by the black points. Especially at high values of η, the upgraded detector design significantly decreases the material budget.

In order to keep the existing power cables and optical fibers and still meet the increased power

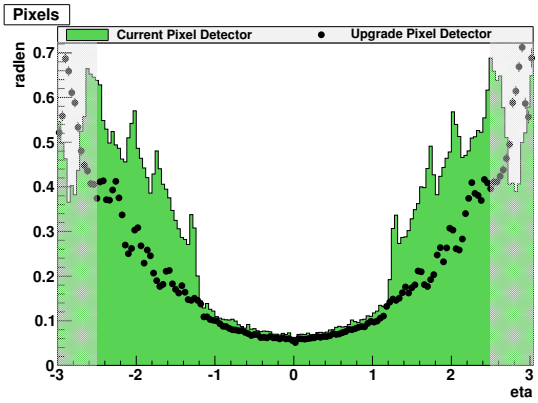

Figure 4: *Left:* The amount of material in the pixel detector shown in units of radiation length as a function of the pseudorapidity η; this is given for the current pixel detector (green histogram), and the Phase I upgraded detector (black points). The shaded region at high $|\eta|$ is outside the region for track reconstruction. *Right:* ultra-lightweight mechanical support structure prototype for BPIX layer 1.

and readout bandwidth requirements of the additional detector layer, DC-DC converters and the digital pixel readout of the upgraded ROC are needed, respectively.

3. Expected Performance of the Upgraded Detector

Improvements from the new detector cannot be summed up by one number, but are characterized by higher efficiencies, lower fake rates, lower dead-time/data-loss, and an extended life time of the detector. In this section, the b-tagging efficiency is discussed as an example for the improved performance of the upgraded detector even in the high pile-up environment of the Phase I operation.

With the expected improvements in the tracking efficiency, track impact parameter resolution, and primary vertex resolutions mentioned in the previous sections, the b-tagging performance of the Phase I upgrade pixel detector is expected to be significantly better than that of the current detector at high pileup.

The performance of the CMS b-tagging algorithms was studied using a sample of simulated $t\bar{t}$ events. Results for the "Combined Secondary Vertex" algorithm [6] are presented. No tuning was done for high pileup or for the upgraded detector on the selection criteria for the track collections used in the algorithms, nor was any tuning done of the b-tagging algorithms themselves.

Figure 5a shows the b-tagging performance with no pileup. The plot shows the fraction of c-jets and (light) dusg-jets that are misidentified as a b-jet as a function of the efficiency for identifying a b-jet correctly as a b-jet. The results show that the b-tagging performance is significantly better for the upgrade pixel detector even at zero pileup when the performance of the current pixel detector is neither degraded by dynamic data loss nor by high hit occupancies. This illustrates the power of both having the extra pixel layer in the upgrade detector and having the innermost layer closer to the interaction point.

It can be seen in figure 5b that the b-tagging performance for the upgrade pixel detector at 2×10^{34} cm^{-2}s^{-1} is superior to the current detector running under pileup conditions similar to the ones present during 2012 data taking with an average pileup of 25.

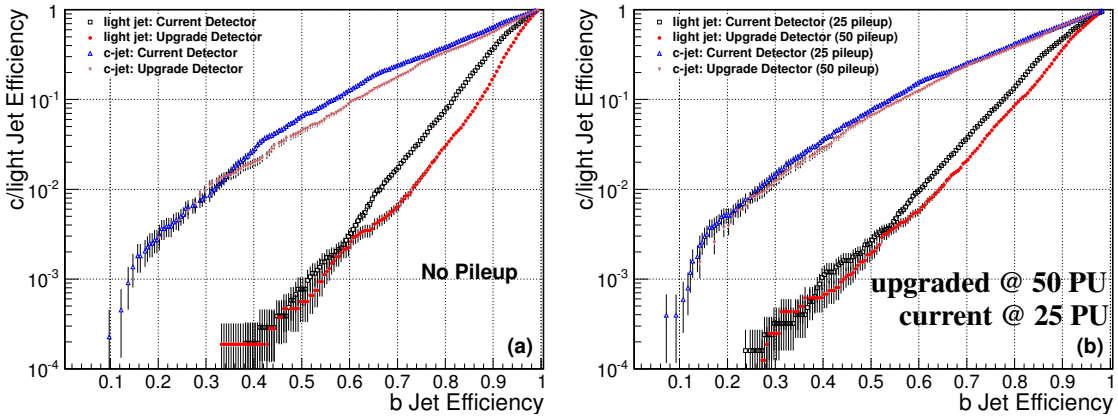

Figure 5: Performance of the Combined Secondary Vertex b-tagging algorithm for jets with $p_T > 30\,\text{GeV}$ in a $t\bar{t}$ Monte Carlo sample with (a) zero pileup (PU) and (b) comparing the current pixel detector at an average PU of 25 with the upgraded detector at a PU of 50. The performance for the current detector is shown by the open markers while the solid markers are for the upgrade detector. The triangular points are for c-jets while the circle and square points are for light quark/gluon jets.

4. Test-beam Studies of Upgraded Read-Out Chip Performance

With the start of the module production foreseen for mid-2014, read-out chip prototypes with the upgraded design have already undergone extensive testing in different testbeams.

In this section, preliminary results of testbeam measurements at DESY using single-ROC modules inside a pixel beam telescope are presented.

4.1 Setup in the Mimosa-based Pixel Beam Telescope at the DESY Testbeam

The performance of the upgraded ROCs was investigated at the DESY positron beam lines which provide up to 1000 particles per cm^2 and second at energies from 1 to 6 GeV.

Single-ROC modules were installed as rotatable device-under-test (DUT) between the two arms of an EUDET/AIDA-family pixel beam telescope [7]. The latter consists of six planes of Mimosa26 MAPS devices [8] which cover an area of $2 \times 1\,\text{cm}^2$ and have been thinned down to 50 µm to reduce multiple scattering of the beam particles. As the Mimosa26 operate in rolling-shutter mode and integrate over $\mathcal{O}(100\,\mu\text{s})$, an additional single-ROC module was placed behind the telescope to provide a timing reference. A trigger was issued to all components of the setup based on the coincidence of four scintillator signals.

With the experimental setup as depicted in figure 6, the track extrapolation error at the DUT position is approximately 4.8 µm for 4 GeV positrons.

4.2 Performance of unirradiated ROCs

Figure 7 shows the column resolution versus the turn angle with the telescope extrapolation uncertainty subtracted. The turn angle corresponds to a rotation around the column axis and maps to the rapidity inside the CMS experiment.

The best column resolution of $\sim 10\,\mu\text{m}$ for the lower threshold of 1.5 ke is reached at the angle where optimal charge sharing between neighboring pixels occurs, i.e. where the particles most

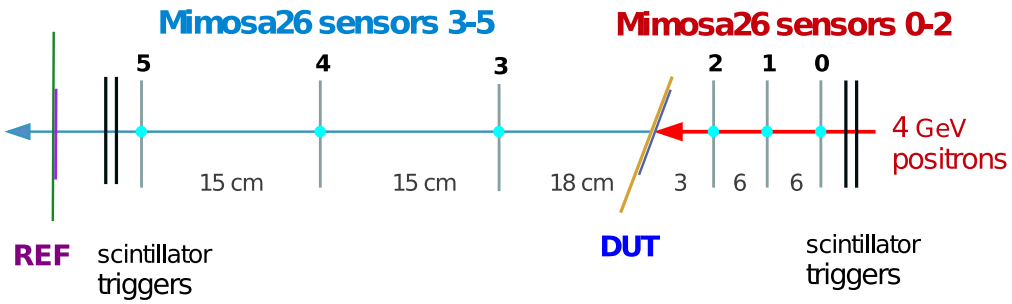

Figure 6: Experimental setup: device-under-test (DUT) in the center of the pixel beam telescope consisting of six Mimosa26 planes, a timing reference plane (REF) behind the telescope, and two scintillator triggers on each side of the telescope.

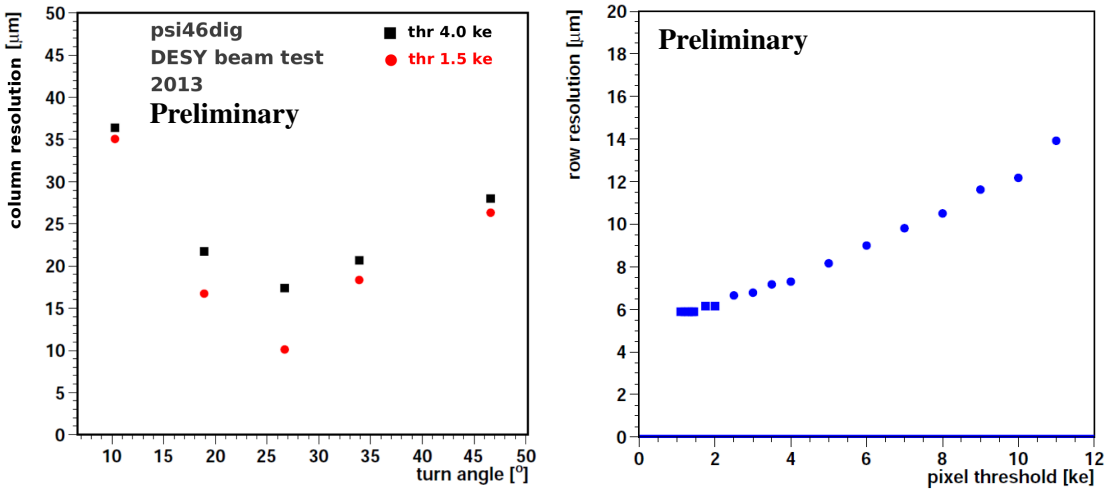

Figure 7: *Left:* Column resolution versus turn angle; *Right:* Row resolution versus threshold at fixed optimal tilt angle of 20°. In both cases, the telescope extrapolation uncertainty has been subtracted.

likely traverse two pixel cells. This optimal angle is determined by the pixel geometry[4] and is 28° in column direction in which the pixels have a width of 150 µm. The difference to the higher threshold of 4.0 ke is also most pronounced at this angle.

This threshold-dependence of the resolution is investigated in more detail in the right of figure 7 where the row resolution is measured as function of the threshold value. The sensor has been tilted[5] around the row axis by 20° to reach optimal results for the pixel geometry in row direction.[6] The telescope extrapolation uncertainty has been subtracted.

The plot shows a significant improvement of the row resolution for lower threshold values which seems to saturate at 6 µm for thresholds below 2 ke. The difference in row resolution be-

[4] atan(pixel width in column direction/sensor thickness) = atan(150 µm/285 µm) ≈ 28°

[5] A tilting rotation maps to the r-ϕ direction in the CMS experiment.

[6] atan(pixel width in row direction/sensor thickness) = atan(100 µm/285 µm) ≈ 20°. This optimal tilt angle corresponds to the value of the Lorentz angle for the pixel barrel modules in the CMS experiment due to charge carrier drift in the magnetic field.

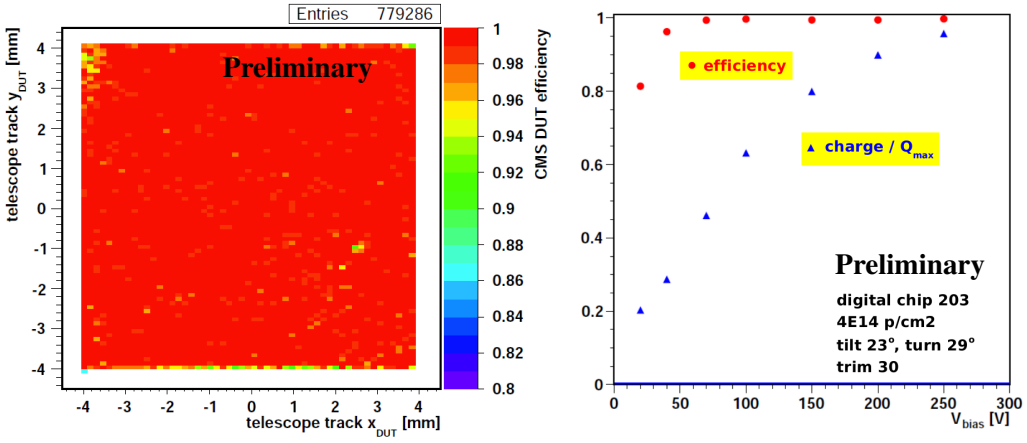

Figure 8: Efficiency pixel map (*left*) and average charge collection (blue triangles) and hit (red circles) efficiencies as function of the bias voltage (*right*) of a single ROC module irradiated at CERN PS, 24 GeV protons, with a fluence of $3.77 \times 10^{14}\,\mathrm{p/cm^2}(\pm 7.6\%)$ which corresponds to Layer 4 after $500\,\mathrm{fb}^{-1}$.

tween threshold values of 4 ke and the lowest value achieved with the new ROC design of 1.5 ke is approximately 2 µm. This demonstrates the expected performance gain of the upgraded ROC with its significantly reduced in-time threshold.

4.3 Performance of ROCs irradiated up to 130 kGy

To verify the performance of the upgraded ROC in the presence of radiation damage, single-ROC modules have been irradiated in the 24 GeV proton beam of CERN PS. The maximum dose of 130 kGy is equivalent to a fluence of $3.77 \times 10^{14}\,\mathrm{p/cm^2}(\pm 7.6\%)$ and corresponds to the expected life time dose after $500\,\mathrm{fb}^{-1}$ of layer 4.

Figure 8 shows preliminary results from testbeam measurements on a single-ROC module irradiated up to 130 kGy and operated at a threshold of 1.5 ke. The left-hand plot shows an *x*-*y* map of the pixels and their hit efficiency as indicated by color. Even though after irradiation the efficiency is typically still above 98% and shows no pattern across the sensor, there are some smaller regions visible where it drops to $\sim 90\%$. These effects are still being investigated but could be attributed to inhomogeneities during the irradiation process.

The right-hand plot of figure 8 shows the average hit efficiency (as red circles) and the charge collection efficiency (as blue triangles) over the whole single-ROC module as function of the applied bias voltage.

At lower bias, the charge collection efficiency quickly drops and reaches values below 50% at voltages less than $\sim 80\,\mathrm{V}$. This is caused by the only partially depleted sensor volume at lower bias. However, as the sensor has undergone type inversion and the charge is collected at the implant side, the hit efficiency remains above 98% down to a bias of $\sim 70\,\mathrm{V}$ where only about half of the maximum charge is collected. For bias voltages below this value, the hit efficiency starts to drop significantly.

This "graceful exit" behavior extends the period in which the pixel detector can be operated efficiently while exposed to increasing radiation damage.

5. Conclusion

The upgrade of the CMS pixel tracker as proposed in [3] is motivated by the excellent performance of LHC to-date and the anticipated future operation as well as the accumulated radiation damage. Due to data losses in the read-out chip, the present system will not sustain the extreme operating conditions expected in Phase I.

An additional detector layer, reduced material budget and improved readout will maintain or even improve the high tracking performance of the current pixel detector at luminosities up to $2 \times 10^{34}\,\mathrm{cm}^{-2}\mathrm{s}^{-1}$ and pile-up up to and exceeding 50.

The improvements of the upgraded detector design are broad and substantial and will have a significant impact on the CMS physics reach.

Preliminary results from testbeam studies on prototypes of the new read-out chip demonstrate the improved performance of the new design and its capability to be operated efficiently even in the presence of radiation damage.

The upgrade will be performed with minimal impact on other detector components during the short time available in the technical stop 2016/2017.

References

[1] CMS Collaboration. The CMS tracker system project: Technical design report. Technical Report CERN-LHCC-98-006, CERN, 1998.

[2] CMS Collaboration. The CMS tracker: addendum to the technical design report. Technical Report CERN-LHCC-2000-016, CERN, 2000.

[3] CMS Collaboration. CMS technical design report for the pixel detector upgrade. Technical Report CERN-LHCC-2012-016. CMS-TDR-011, CERN, Geneva, Sep 2012.

[4] T. Rohe, A. Bean, V. Radicci, and J. Sibille. Planar sensors for the upgrade of the CMS pixel detector. *Nucl.Instrum.Meth.A*, A650:136–139, 2011.

[5] Hans-Christian Kästli. CMS pixel upgrade project. In *VERTEX2010*, volume 039. PoS, 2010.

[6] Christian Weiser. A combined secondary vertex based b-tagging algorithm in CMS. Technical Report CMS-NOTE-2006-014, CERN, Geneva, Jan 2006.

[7] EUDET Consortium. Detector research and development towards the International Linear Collider. final report, 2011.

[8] C. Hu-Guo, J. Baudot, G. Bertolone, A. Besson, A.S. Brogna, C. Colledani, G. Claus, R. De Masi, Y. Degerli, A. Dorokhov, G. Doziere, W. Dulinski, X. Fang, M. Gelin, M. Goffe, F. Guilloux, A. Himmi, K. Jaaskelainen, M. Koziel, F. Morel, F. Orsini, M. Specht, Q. Sun, O. Torheim, I. Valin, and M. Winter. First reticule size MAPS with digital output and integrated zero suppression for the EUDET-JRA1 beam telescope. *Nucl.Instrum.Meth.A*, 623(1):480 – 482, 2010.